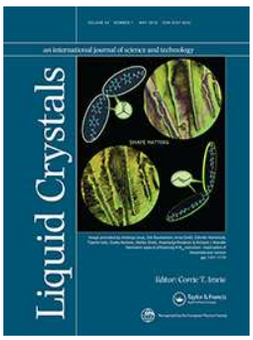

Liquid Crystals

ISSN: 0267-8292 (Print) 1366-5855 (Online) Journal homepage: http://www.tandfonline.com/loi/tlct20

Computational modelling of tactoid dynamics in chromonic liquid crystals

Chiqun Zhang, Amit Acharya, Noel J. Walkington & Oleg D. Lavrentovich

To cite this article: Chiqun Zhang, Amit Acharya, Noel J. Walkington & Oleg D. Lavrentovich (2018) Computational modelling of tactoid dynamics in chromonic liquid crystals, Liquid Crystals, 45:7, 1084-1100, DOI: 10.1080/02678292.2017.1410240

To link to this article: https://doi.org/10.1080/02678292.2017.1410240

Published online: 13 Dec 2017.

LIQUID CRYSTALS, 2018
VOL. 45, NO. 7, 1084–1100
https://doi.org/10.1080/02678292.2017.1410240

Taylor & Francis
Taylor & Francis Group

Computational modelling of tactoid dynamics in chromonic liquid crystals

Chiqun Zhang[a], Amit Acharya[b], Noel J. Walkington[c] and Oleg D. Lavrentovich[d]

[a]Department of Civil and Environmental Engineering, Carnegie Mellon University, Pittsburgh, PA, USA; [b]Department of Civil and Environmental Engineering, and Center for Nonlinear Analysis, Carnegie Mellon University, Pittsburgh, PA, USA; [c]Department of Mathematical Sciences, and Center for Nonlinear Analysis, Carnegie Mellon University, Pittsburgh, PA, USA; [d]Chemical Physics Interdisciplinary Program, and The Liquid Crystal Institute, Kent State University, Kent, OH, USA

ABSTRACT

Motivated by recent experiments, the isotropic–nematic phase transition in chromonic liquid crystals is studied. As temperature decreases, nematic nuclei nucleate, grow and coalesce, giving rise to tactoid microstructures in an isotropic liquid. These tactoids produce topological defects at domain junctions (disclinations in the bulk or point defects on the surface). We simulate such tactoid equilibria and their coarsening dynamics with a model using degree of order, a variable length director and an interfacial normal as state descriptors. We adopt Ericksen's work and introduce an augmented Oseen–Frank energy, with non-convexity in both interfacial energy and the dependence of the energy on the degree of order. A gradient flow dynamics of this energy does not succeed in reproducing some simple expected feature of tactoid dynamics. Therefore, a strategy is devised based on continuum kinematics and thermodynamics to represent such features. The model is used to predict tactoid nucleation, expansion and coalescence during the process of phase transition. We reproduce observed behaviours in experiments and perform an experimentally testable parametric study of the effect of bulk elastic and tactoid interfacial energy parameters on the interaction of interfacial and bulk fields in the tactoids.

ARTICLE HISTORY
Received 23 August 2017
Accepted 23 November 2017

KEYWORDS
Tactoids; lyotropic chromonics; computational modelling; phase transition

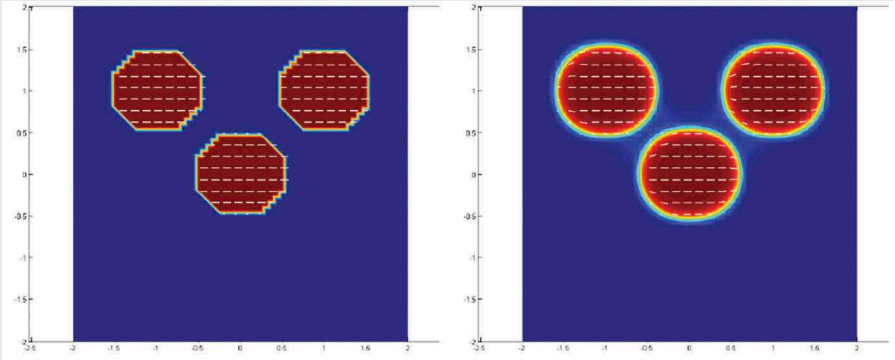

(a) The initialized tactoid shape and director field. Three spherical tactoids with same director fields are initialized.

(b) The tactoid shapes and director field at $t = 0.1$. Three tactoids expand.

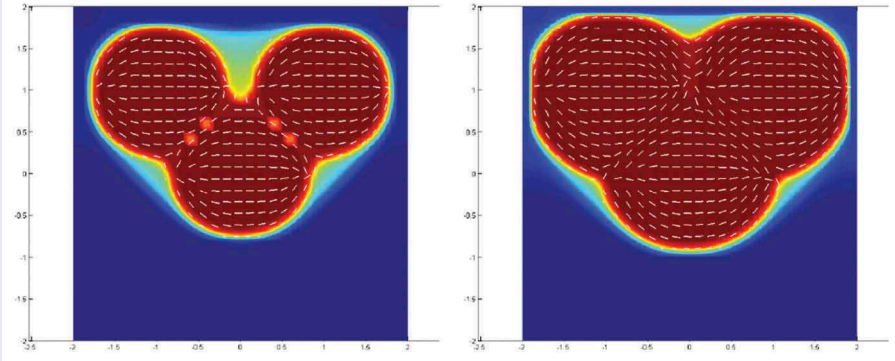

(c) The tactoid shapes and director field at $t = 0.2$. The tactoids begin to merge.

(d) The tactoid shapes and director field at $t = 0.5$. a strength -1 disclination is formed inside the bulk.

CONTACT Amit Acharya acharyaamit@cmu.edu

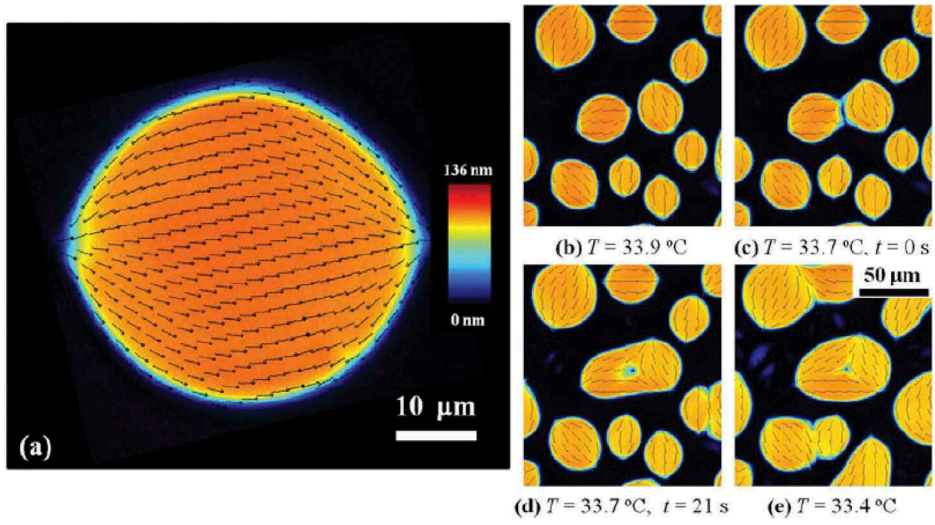

Figure 1. Experiment observations of isotropic–nematic phase transition from Ref. [1].

1. Introduction

Liquid crystals (LCs) are a state of matter with long-range orientational order and complete (nematic) or partial (smectics, columnar phases) absence of long-range positional order of 'building units' (molecules, viruses, aggregates etc.). LCs can flow like viscous liquids and also possess features that are characteristic of solid crystals, such as elasticity and birefringence. In the simplest liquid crystalline phase, called the nematic, the molecules have no positional order but tend to point in the same direction. In this work, we focus on a nematic lyotropic LC (lyotropic chromonic liquid crystal (LCLC)) that possesses a broad biphasic region of coexisting nematic and isotropic phases [1].

LCLCs are formed by water-based dispersions of organic molecules, see the recent reviews [2–4]. The molecules are of a rigid disc-like or plank-like shape with polar groups at the periphery. Once in water, they form elongated aggregates by stacking on top of each other. The aggregates elongate as the concentration is increased and the temperature is reduced, which allows one to trigger phase transitions in the system by changing either the temperature or concentration [5,6]. In particular, the temperature changes can trigger a first order isotropic–nematic (I–N) phase transition of the LCLC. As the temperature increases, the nematic LC loses orientational order and transits to the isotropic phase, with molecular aggregates being short and oriented randomly. On the contrary, if the temperature decreases, the isotropic phase transits to the nematic phase. Both phase transitions occur through nucleation of the so-called tactoids, representing inclusions of one phase in the other [1,7–9]. Tactoids of the nematic phase nucleating upon cooling are called positive tactoids [8] and are the subject of the present work. Tactoids of the isotropic phase nucleating in the nematic background upon heating are called negative tactoids [8]. If the temperature is fixed in the range in which the two phases coexist, these tactoids expand and merge. The uniaxial nematic phase allows three types of topologically stable defects: linear disclinations, point defects hedgehogs and point defect boojums; the latter can exist only at the surface of the nematic [10–13]. In confined volumes, such as droplets and tactoids, some of the topological defects correspond to the equilibrium state of the system, thanks to the anisotropic surface tension that sets a well-defined angle between the director and the normal to the interface [14].

The principal objectives of this work are to

- derive a practical equation of evolution for the degree of orientation based on kinematics and thermodynamics;
- introduce a dynamic model for the nematic–isotropic phase transition of LCLC with an augmented Oseen–Frank energy and non-convex interfacial energy;
- demonstrate the capability of the proposed dynamical model by analysing the results of static equilibrium and the dynamic behaviours.

The main experimental observations and applications of LCLC and their computation are reviewed in Refs. [1–4]. Currently, there is an extensive database on the principal material parameters of the LCLCs and defects in them. All three bulk elastic constants (for splay K_{11}, twist K_{22} and bend K_{33}) have been measured for two main representatives of LCLCs

[15–17]. It was found that the elastic constants of bend and splay can be tuned in a broad range, from a few pN to 70 pN, by changing temperature or the chemical composition of the system (e.g. by adding salts [17]). The director of LCLCs can align either parallel to the interface with an adjacent medium [18] or in a perpendicular fashion, with possible transitions between these two states [19]. At the interface with its own isotropic melt, the director of a nematic LCLC aligns parallel to it [7]. The interfacial surface tension at the I–N interface was estimated to be on the order of 10^{-4} J/m^2 [1]. The defect cores of disclinations in LCLCs extend over long distances (microns and even tens of microns), much larger than the cores of disclinations in thermotropic LCs [20].

In this work, we are primary interested in the observations reported in Ref. [1] to develop a model for understanding the behaviour of tactoids during the I–N transformation. The I–N interface in LCLC favours the director to be tangential to the tactoid interface. Figure 1 shows the experimental observations of the I–N phase transition from Ref. [1]. Figure 1(a) shows a single tactoid, where the black colour represents the isotropic phase while the orange colour represents the nematic phase. The black arrows inside the tactoid represent the director field. Nontrivial morphologies of tactoids with surface cusps and director fields are observed. Due to the surface anisotropy, cusps are associated with surface defects called boojums, as shown in Figure 1(a). Figure 1(b–e) represents the phase transition process from the isotropic to the nematic phase, where the nematic tactoids expand and merge. Merging tactoids often produce disclinations via the Kibble mechanism [11,12,21], as shown in Figure 1(e), where a strength $-\frac{1}{2}$ disclination is formed at the point where tactoids merge. In addition, integer strength disclinations are stable only when their cores constitute a large isotropic inclusion; otherwise, as demonstrated experimentally and analytically by Kim et al. [1] and numerically in Ref. [22], the integer strength disclinations split into pairs of half-integer ones. The motion of an interface between a nematic LC phase and the isotropic phase is investigated with a Ginzburg–Landau equation in Ref. [23]. The confinement of the director field for a spherical particle that explains the observation of a Saturn ring is studied in Ref. [24].

In studies of nematic LCs, a classical convention is to represent the local orientational order by a unit-length director field [25,26]. Oseen and Frank developed an energy density of nematic LCs, with constants representing different director deformations [27,28]. The existence and partial regularity theory of some boundary-value problems based on Oseen–Frank energy density are discussed in Ref. [29]. The Oseen–Frank energy can be augmented by adding an additional surface energy density to represent the interaction between the LC and an adjacent medium; a common form of such a surface energy density is the Rapini–Papoular surface energy.

In this paper, we develop a computational model for the I–N phase transition accounting for interfacial energy as an enhancement of Ericksen's variable degree of order $(s,\boldsymbol{n})$ model [26]. We introduce the pair $(s,\boldsymbol{d})$ with $(\boldsymbol{d} = s\boldsymbol{n})$. The state variable s has the meaning of the degree of order parameter in Ericksen's model [26] and $\boldsymbol{d}$ serves for the director whose magnitude is constrained to be equal to $|s|$. Thus, the director is of unit length in the nematic phase, it vanishes in the isotropic phase, and it is of variable length at interfaces between the two phases. This practical device of replacing $\boldsymbol{n}$ by $\boldsymbol{d}$ is essential in terms of having a setting that is well posed for computations of a time-dependent non-linear theory, since leaving the value of the director field undefined in parts of the domain, that furthermore evolve in time, does not lead to unique evolution and simply cannot be practically implemented.

The rest of this paper is organised as follows: In Section 2, we outline our notation and terminology. In Section 3, a dynamic model for the phase transition process based on kinematics as well as thermodynamics is derived. In Section 4, the results of equilibrium and dynamic behaviours are shown and discussed. The significance of the dynamic model is demonstrated and explained. In Section 5, we report on a preliminary parametric study of material constants in the model. We end with some concluding remarks in Section 6.

2. Notation and terminology

The condition that a is defined to be b is indicated by the statement $a := b$. The Einstein summation convention is implied unless specified otherwise. The symbol $\boldsymbol{A}\boldsymbol{b}$ denotes the action of a tensor $\boldsymbol{A}$ on a vector $\boldsymbol{b}$, producing a vector. In the sequel, $\boldsymbol{a}\cdot\boldsymbol{b}$ represents the inner product of two vectors $\boldsymbol{a}$ and $\boldsymbol{b}$; the symbol $\boldsymbol{A}\boldsymbol{B}$ represents tensor multiplication of the second-order tensors $\boldsymbol{A}$ and $\boldsymbol{B}$.

The symbol div represents the divergence and grad represents the gradient. In this paper, all tensor or vector indices are written with respect to the basis e_i, i = 1–3, of a rectangular Cartesian coordinate system. The following component-form notation holds

$$\begin{aligned}(\boldsymbol{a}\times\boldsymbol{b})_i &= e_{ijk}a_jb_k\\ (\text{curl }\boldsymbol{a})_i &= e_{ijk}a_{k,j}\\ (\text{div }\boldsymbol{A})_i &= A_{ij,j}\\ (\boldsymbol{A}:\boldsymbol{B}) &= A_{ij}B_{ij}\end{aligned}$$

where e_{mjk} is a component of the alternating tensor $\boldsymbol{X}$.

The following list describes some of the mathematical symbols we use in this work:

- $\boldsymbol{n}$: the unit vector field representing the director;
- s: the degree of orientation, $s=0$ represents the isotropic phase while $s=1$ represents the nematic phase;
- $\boldsymbol{d}$: the alternative vector field representing the director with $\boldsymbol{d}=s\boldsymbol{n}$ and
- ψ: the free energy density.

3. Derivation of dynamic model

3.1. s Evolution equation in Ericksen–Leslie model

In Ref. [26], Ericksen introduced a variable degree of orientation s to represent different phase states of a LC. In his model, $s=0$ represents the isotropic phase and $s=1$, the nematic phase. Also, a unit length vector field is introduced to represent the director field, denoted as $\boldsymbol{n}$. In Ericksen's model, the balance law to derive the s evolution equation is given as

$$\dot{P}=\text{div}\,(\boldsymbol{T})+G^I+G^E,$$

where ψ is free energy density, P is a generalised momentum with $P=\partial\psi/\partial s$, $\boldsymbol{T}$ is a generalised stress, G^I represents a kind of internal body force with $G^I=-\partial\psi/\partial s+\hat{G}$ and G^E is an external effect. Assuming the free energy density, ψ depends on $(s,\text{grad }s,\boldsymbol{n},\text{grad }\boldsymbol{n})$, and following the argument in Ref. [26], we have

$$\frac{\overset{\cdot}{\partial\psi}}{\partial s}=\text{div}\left(\frac{\partial\psi}{\partial\,\text{grad }s}\right)-\frac{\partial\psi}{\partial s}+\hat{G}+G^E$$

$$\Rightarrow\frac{\partial^2\psi}{\partial s^2}\dot{s}+\frac{\partial^2\psi}{\partial s\partial\,\text{grad }s}\cdot\frac{\cdot}{\text{grad }s}+\frac{\partial^2\psi}{\partial s\partial n}\cdot\dot{\boldsymbol{n}}+\frac{\partial^2\psi}{\partial s\partial\,\text{grad }\boldsymbol{n}}:\frac{\cdot}{\text{grad }\boldsymbol{n}}=\text{div}\left(\frac{\partial\psi}{\partial\,\text{grad }s}\right)-\frac{\partial\psi}{\partial s}+\hat{G}+G^E.$$

After rearranging the terms, s evolution equation in Ericksen's model can be written as

$$\left(\frac{\partial^2\psi}{\partial s^2}\right)\dot{s}+\frac{\partial^2\psi}{\partial s\partial\,\text{grad }s}\cdot\frac{\cdot}{\text{grad }s}=$$

$$\text{div}\left(\frac{\partial\psi}{\partial\,\text{grad }s}\right)-\frac{\partial\psi}{\partial s}+\hat{G}+G^E-\frac{\partial^2\psi}{\partial s\partial\boldsymbol{n}}\cdot\dot{\boldsymbol{n}}-\frac{\partial^2\psi}{\partial s\partial\,\text{grad }n}:\frac{\cdot}{\text{grad }\boldsymbol{n}}.$$

In this work, we would like to adopt a simpler evolution statement since the fundamental basis for Ericksen's balance law $\dot{P}=\text{div}\,(\boldsymbol{T})+G^I+G^E$ is not clear to us. In particular, the coefficient $\frac{\partial^2\psi}{\partial s^2}$ may change sign as the dependence on s of the energy is non-convex.

3.2. Motivation and derivation of s evolution

We derive a practical model for tactoid and I–N phase transition dynamics based on continuum kinematics and thermodynamics. To get the evolution equation for s, suppose there is a level set of s with normal velocity field $\boldsymbol{V}^{(s)}$ along it, travelling from $\boldsymbol{x}_2$ to $\boldsymbol{x}_1$ during a time interval Δt, as shown in Figure 2. The time derivative of s at $\boldsymbol{x}_1$ and t is

$$\frac{\partial s}{\partial t}(\boldsymbol{x}_1,t)=\lim_{\Delta t\to 0}\frac{s(\boldsymbol{x}_1,t+\Delta t)-s(\boldsymbol{x}_1,t)}{\Delta t}. \tag{1}$$

Since the level set of s travels from $\boldsymbol{x}_2(\Delta t)$ to $\boldsymbol{x}_1:=\boldsymbol{x}_2(\Delta t=0)$, $\Delta t>0$, during the time interval Δt, $s(\boldsymbol{x}_1,t+\Delta t)=s(\boldsymbol{x}_2(\Delta t),t)$. Thus, $\frac{\partial s}{\partial t}$ may also be expressed as

$$\frac{\partial s}{\partial t}(\boldsymbol{x}_1,t)=\lim_{\Delta t\to 0}\frac{s(\boldsymbol{x}_2(\Delta t),t)-s(\boldsymbol{x}_1,t)}{\Delta t}. \tag{2}$$

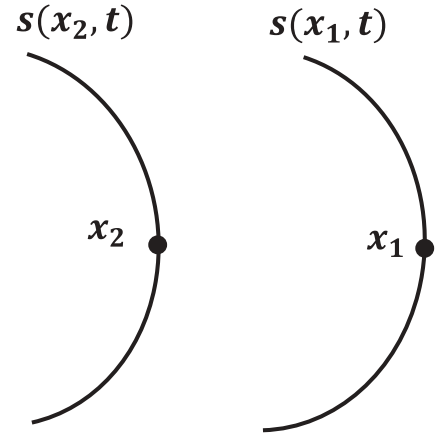

Figure 2. A level set of s moving from x_2 to x_1 during Δt.

Assuming s is differentiable in its arguments and writing the derivative in the first argument as grad s, we have

$$\begin{aligned} s(\boldsymbol{x}_2(\Delta t),t)-s(\boldsymbol{x}_1,t) &= \text{grad } s(\boldsymbol{x}_1,t)[\boldsymbol{x}_2(\Delta t)-\boldsymbol{x}_1] \\ &+ o(\boldsymbol{x}_2(\Delta t)-\boldsymbol{x}_1) \Rightarrow \frac{s(\boldsymbol{x}_2(\Delta t),t)-s(\boldsymbol{x}_1,t)}{\Delta t} \\ &= \text{grad } s(\boldsymbol{x}_1,t)\frac{1}{\Delta t}[\boldsymbol{x}_2(\Delta t)-\boldsymbol{x}_1]+\frac{1}{\Delta t}o(\boldsymbol{x}_2(\Delta t)-\boldsymbol{x}_1). \end{aligned} \tag{3}$$

Substitute Equation (3) in Equation (2), we have

$$\begin{aligned} \frac{\partial s}{\partial t}(\boldsymbol{x}_1,t) &= \text{grad } s(\boldsymbol{x}_1,t)\lim_{\Delta t\to 0}\frac{\boldsymbol{x}_2(\Delta t)-\boldsymbol{x}_1}{\Delta t} \\ &+ \lim_{\Delta t\to 0}\frac{o(\boldsymbol{x}_2(\Delta t)-\boldsymbol{x}_1)}{\Delta t}. \end{aligned} \tag{4}$$

Denote $\boldsymbol{V}^{(s)}$ as the velocity of movement of a level set of s, $\boldsymbol{V}^{(s)}=\lim_{\Delta t\to 0}\frac{\boldsymbol{x}_1-\boldsymbol{x}_2(\Delta t)}{\Delta t}$. Since

$$\begin{aligned} \lim_{\Delta t\to 0}\left|\frac{o(\boldsymbol{x}_2(\Delta t)-\boldsymbol{x}_1)}{\Delta t}\right| &= \lim_{\Delta t\to 0}\frac{|o(\boldsymbol{x}_2(\Delta t)-\boldsymbol{x}_1)|}{|\boldsymbol{x}_2(\Delta t)-\boldsymbol{x}_1|}\frac{|\boldsymbol{x}_2(\Delta t)-\boldsymbol{x}_1|}{\Delta t} \\ &= -0\cdot\left|\boldsymbol{V}^{(s)}\right|=0, \end{aligned}$$

(4) becomes

$$\frac{\partial s}{\partial t}=-\text{grad } s\cdot\boldsymbol{V}^{(s)}.$$

If the material velocity is v and the change in the value of s at $\boldsymbol{x}_1$ arises from factors more than the pure advection of the value of s from $\boldsymbol{x}_2$ to $\boldsymbol{x}_1$ due to material motion, then we assign the rest of this change as occurring due to the progress of the phase transition front. In general, we can decompose $\boldsymbol{V}^{(s)}=\boldsymbol{v}+\boldsymbol{V}$, where $\boldsymbol{V}$ is the phase front velocity relative to the material and $\boldsymbol{v}$ is the material velocity. Recall that the material time derivative of s is defined as

$$\dot{s}:=\frac{ds}{dt}=\frac{\partial s}{\partial t}+\text{grad } s\cdot\boldsymbol{v};$$

therefore, the s evolution is given as

$$\dot{s}=-\text{grad}\, s\cdot\boldsymbol{V}. \tag{5}$$

In particular, there are two special cases:

- Suppose this velocity was purely due to s being transported by the material velocity $\boldsymbol{v}$. Then, we have $\dot{s}=\frac{\partial s}{\partial t}+\frac{\partial s}{\partial \boldsymbol{x}}\cdot\boldsymbol{v}=0$.
- If there is no material velocity but transport is only due to motion of the phase front, then $\boldsymbol{V}^{(s)}$ is just the speed of the phase front transition $\boldsymbol{V}$.

To get an explicit form of the phase front velocity $\boldsymbol{V}$, assume the free energy density per unit mass takes the form $\psi(\boldsymbol{n},\text{grad }\boldsymbol{n},s,\text{grad } s)$. Following Refs. [30,31], take the external power as

$$P(t)=\int_{\partial V}(\boldsymbol{\Lambda}\mathrm{v})\cdot\omega da+\int_V\rho\boldsymbol{K}\cdot\omega dv,$$

where $\boldsymbol{\Lambda}$ is the couple stress tensor, $\boldsymbol{K}$ is the external body moment per unit mass, $\boldsymbol{v}$ is the unit normal vector on the boundary of the body and ω is the director angular velocity (we have ignored material motion for simplicity). Applying the divergence theorem, we have

$$\begin{aligned} \int_{\partial V}(\boldsymbol{\Lambda}\boldsymbol{v})\cdot\omega da &= \int_{\partial V}\Lambda_{ij}\omega_i\mathrm{v}_j da \\ &= \int_V(\Lambda_{ij,j}\omega_i+\Lambda_{ij}\omega_{i,j})dv. \end{aligned}$$

Thus, the external power P can be written as

$$P(t)=\int_V[\text{div }\boldsymbol{\Lambda}+\rho\boldsymbol{K}]\cdot\omega dv+\int_V\boldsymbol{\Lambda}:\boldsymbol{M}dv,$$

where $\boldsymbol{M}$ is defined as director angular velocity gradient $\boldsymbol{M}=\text{grad}\,\omega$. Recall that the balance law of angular momentum reads as

$$\text{div}\,\boldsymbol{\Lambda}+\rho\boldsymbol{K}=0,$$

leading to

$$P(t)=\int_V\boldsymbol{\Lambda}:\boldsymbol{M}\,dv.$$

In addition, the second law of thermodynamics requires the dissipation to be equal or larger than zero, which is given as

$$\int_V[\boldsymbol{\Lambda}:M]-\rho\dot{\psi}]\,dv\geq 0 \tag{6}$$

$$\Rightarrow\int_V\left[\Lambda_{ij}\omega_{i,j}-\rho\frac{\partial\psi}{\partial n_i}\dot{n}_i-\rho\frac{\partial\psi}{\partial(n_{i,j})}\dot{n}_{i,j}-\rho\frac{\partial\psi}{\partial s}\dot{s}-\rho\frac{\partial\psi}{\partial(s_{,j})}\dot{s}_{,j}\right]dv \geq 0.$$

As flow is ignored for the moment, the inequality takes the form

$$\int_V\left[\Lambda_{ij}\omega_{i,j}-\rho\frac{\partial\psi}{\partial n_i}\dot{n}_i-\rho\frac{\partial\psi}{\partial(n_{i,j})}\dot{n}_{i,j}-\rho\frac{\partial\psi}{\partial s}\dot{s}-\rho\frac{\partial\psi}{\partial(s_{,j})}\dot{s}_{,j}\right]dv \geq 0$$

$$\begin{aligned} \Rightarrow\int_V\Bigg[&\Lambda_{ij}\omega_{i,j}-\rho\frac{\partial\psi}{\partial n_i}(\omega\times n)_i-\rho\frac{\partial\psi}{\partial(n_{i,j})}(\omega\times n)_{i,j} \\ &-\rho\frac{\partial\psi}{\partial s}\dot{s}+\rho\left(\frac{\partial\psi}{\partial(s_{,j})}\right)_{,j}\dot{s}\Bigg]dv \\ &-\int_{\partial V}\rho\frac{\partial\psi}{\partial(s_{,j})}\dot{s}\mathrm{v}_j da\geq 0. \end{aligned}$$

Defining the couple stress $\boldsymbol{\Lambda}$ as

$$\boldsymbol{\Lambda}_{ij} := \rho e_{inm} n_n \frac{\partial \psi}{\partial n_{m,j}},$$

and applying the Ericksen identity [32] as

$$\left(\frac{\partial \psi}{\partial n} \otimes n + \frac{\partial \psi}{\partial \operatorname{grad} n}(\operatorname{grad} n) + \left(\frac{\partial \psi}{\partial \operatorname{grad} n}\right) \operatorname{grad} n\right)_{skew} = 0,$$

we obtain

$$\Lambda_{ij}\omega_{i,j} - \rho \frac{\partial \psi}{\partial n_i}(\omega \times n)_i - \rho \frac{\partial \psi}{\partial (n_{i,j})}(\omega \times n)_{i,j} = 0.$$

Then, the dissipation inequality becomes

$$\int_V \left[-\rho \frac{\partial \psi}{\partial s}\dot{s} + \rho \left(\frac{\partial \psi}{\partial (s_{,j})}\right)_{,j} \dot{s}\right] dv - \int_{\partial V} \rho \frac{\partial \psi}{\partial (s_{,j})} \dot{s} \nu_j da \geq 0. \tag{7}$$

To fulfil this inequality, recalling Equation (5) that $\dot{s} = -\operatorname{grad} s \cdot \boldsymbol{V}$, one requires

$$-\left[\rho \frac{\partial \psi}{\partial s} - \rho \left(\frac{\partial \psi}{\partial (s_{,j})}\right)_{,j}\right] s_{,i} V_i \geq 0 \quad \text{at interior points}$$

$$-\rho \frac{\partial \psi}{\partial (s_{,j})} \nu_j s_{,i} V_i \geq 0 \quad \text{at points on boundary.}$$

Therefore, the choice of $\boldsymbol{V}^B$ on the boundary pointing in the direction of

$$-\rho \left(\frac{\partial \psi}{\partial (\operatorname{grad} s)} \cdot \boldsymbol{\nu}\right) \operatorname{grad} s,$$

and $\boldsymbol{V}^I$ in the interior pointing in the direction of

$$-\left[\rho \frac{\partial \psi}{\partial s} - \rho \operatorname{div}\left(\frac{\partial \psi}{\partial (\operatorname{grad} s)}\right)\right] \operatorname{grad} s$$

satisfy the non-negative dissipative requirement. In particular, $\boldsymbol{V}^I$ in the interior may be further assumed as

$$\boldsymbol{V}^I = -\frac{\operatorname{grad} s}{B_m |\operatorname{grad} s|^m}\left[-\rho \operatorname{div}\left(\frac{\partial \psi}{\partial (\operatorname{grad} s)}\right) + \rho \frac{\partial \psi}{\partial s}\right].$$

where B_m is a material constant required on dimensional grounds related to 'drag', and m is a parameter representing different scenarios, which can be 0, 1 and 2. With $\dot{s} = -\operatorname{grad} s \cdot V$, the evolution equation of s can be written as

$$\dot{s} = \frac{1}{B_m} |\operatorname{grad} s|^{2-m} \rho \left[-\frac{\partial \psi}{\partial s} + \operatorname{div}\left(\frac{\partial \psi}{\partial (\operatorname{grad} s)}\right)\right]. \tag{8}$$

$m = 0$ is the *simplest* natural choice representing a linear kinetic assumption. $m = 2$ corresponds to the evolution equation derived from the gradient flow method. To this is appended the balance laws of linear momentum and angular momentum, utilising the constitutive equations for couple stress and stress, the latter arising from the thermodynamic procedure above when flow is included [33].

Another way to obtain the s evolution equation is the gradient flow method. The gradient flow dynamics (for a non-conserved quantity) assumes that all information on evolution is directly available (up to a material parameter) once the energy function is known. Consider the total energy

$$E = \int_V \rho \psi(\boldsymbol{n}, \operatorname{grad} \boldsymbol{n}, s, \operatorname{grad} s)\, dv.$$

The first variation of the energy E is

$$\delta E = \int_V \left(\frac{\partial \psi}{\partial \boldsymbol{n}} \cdot \delta \boldsymbol{n} + \frac{\partial \psi}{\partial \operatorname{grad} \boldsymbol{n}} : \delta(\operatorname{grad} \boldsymbol{n}) + \frac{\partial \psi}{\partial s}\delta s + \frac{\partial \psi}{\partial \operatorname{grad} s} \cdot \delta(\operatorname{grad} s)\right) dv.$$

Integrate by parts the term involving $\delta(grad\ s)$ to obtain the s evolution equation based on an L^2 gradient flow as

$$\dot{s} = \gamma \left[\operatorname{div} \frac{\partial \psi}{\partial \operatorname{grad} s} - \frac{\partial \psi}{\partial s}\right], \tag{9}$$

where γ is a dimensional constant. The result from the energy gradient flow method is equivalent to the evolution equation given in Equation (8) for $m = 2$.

3.3. Phase transition model formulation

In Ericksen's model [26], the director field is represented by a unit length vector field n. To practically implement the computation of a time-dependent non-linear theory, we adopt an alternative vector field $\boldsymbol{d}$ to represent the director field subject to the constraint $|\boldsymbol{d}|^2 = \boldsymbol{s}^2$.

Assuming the generalised Parodi relation, the governing equations are an extension of the work in Ref. [34] and take the form

$$\begin{aligned}
&\rho \dot{\boldsymbol{v}} + \operatorname{grad} p - \operatorname{div}\left(\frac{\partial R}{\partial \operatorname{grad} \boldsymbol{v}} - (\operatorname{grad} \boldsymbol{d})^T \frac{\partial W}{\partial \operatorname{grad} \boldsymbol{d}} - (\operatorname{grad} s) \otimes \frac{\partial W}{\partial \operatorname{grad} s}\right) = \rho \boldsymbol{f} \\
&\frac{\partial R}{\partial \dot{\boldsymbol{d}}} + \frac{\partial W}{\partial \boldsymbol{d}} - \operatorname{div}\left(\frac{\partial W}{\partial \operatorname{grad} \boldsymbol{d}}\right) + \lambda \boldsymbol{d} = \rho \boldsymbol{m} \\
&\frac{\partial R}{\partial \dot{s}} + \frac{\partial W}{\partial s} - \operatorname{div}\left(\frac{\partial W}{\partial \operatorname{grad} s}\right) - \lambda s = \rho f_s
\end{aligned} \tag{10}$$

where ρ is the material density, p and λ are Lagrange multipliers dual to the constraints

$$\operatorname{div}(v) = 0 \quad \text{and} \quad |\boldsymbol{d}|^2 - s^2 = 0,$$

W is a modified Oseen–Frank energy and R is an appropriately designed dissipation function.

We introduce the modified Oseen–Frank energy as

$$\begin{aligned} W(\boldsymbol{d}, \operatorname{grad} \boldsymbol{d}, s, \operatorname{grad} s) &= \frac{k_1}{2} \operatorname{div}(\boldsymbol{d})^2 + \frac{k_2}{2} (\boldsymbol{d} \cdot \operatorname{curl}(\boldsymbol{d}))^2 \\ &+ \frac{k_2 - k_4}{2} (|\operatorname{grad} \boldsymbol{d}|^2 - \operatorname{div}(\boldsymbol{d})^2 - |\operatorname{curl}(d)|^2) \\ &+ \frac{k_3}{2} |d \times \operatorname{curl}(\boldsymbol{d})|^2 \\ &+ \frac{L_1}{2} |\operatorname{grad} s|^2 + f(s) + g(\operatorname{grad} s, \boldsymbol{d}), \end{aligned} \tag{11}$$

where k_1, k_2, k_3 and k_4 correspond to the Frank constants, L_1 is the Leslie parameter and $f(s)$ is a non-convex function of s indicating the preferred phase state. The $(s, \boldsymbol{d})$ modified Oseen–Frank energy function has been further augmented by the function $g(\operatorname{grad} s, \boldsymbol{d})$ which is a non-convex function representing interfacial energy. A natural candidate for $g(\operatorname{grad} s, \boldsymbol{d})$ is given as

$$g(\operatorname{grad} s, \boldsymbol{d}) = |\operatorname{grad} s| \left[\sigma_0 \left(1 + w \frac{(\operatorname{grad} s \cdot \boldsymbol{d})^2}{|\operatorname{grad} s|^2 |\boldsymbol{d}|^2} \right) \right], \tag{12}$$

where σ_0 is an isotropic interfacial energy and w is the anchor coefficient [1]. This is an adaptation of the Rapini–Papoular function [35]. The analogue of the Parodi condition has Raleighian

$$\begin{aligned} R = (\gamma_0/2)(\boldsymbol{d} \cdot \boldsymbol{D}\boldsymbol{d})^2 + (\hat{\gamma}_2/2)|\boldsymbol{d} \otimes \boldsymbol{D}\boldsymbol{d}|^2 \\ + (\gamma_1/2)|\overset{\circ}{\boldsymbol{d}}|^2 + \gamma_2 \overset{\circ}{\boldsymbol{d}} \cdot \boldsymbol{D}\boldsymbol{d} + \beta_1 \dot{s} \boldsymbol{d} \cdot \boldsymbol{D}\boldsymbol{d} + (\beta_2/2)\dot{s}^2, \end{aligned}$$

where $\overset{\circ}{\boldsymbol{d}} := \boldsymbol{R}^* \frac{d}{dt}(\boldsymbol{R}^{*T} \boldsymbol{d}) = \dot{\boldsymbol{d}} - \boldsymbol{\Omega}\boldsymbol{d}$ is the convected derivate of $\boldsymbol{d}$ with respect to $\boldsymbol{R}^*$ (also called the Jaumann derivative) and $\boldsymbol{R}^*$ satisfies $\boldsymbol{R}^* \boldsymbol{R}^{*T} = \boldsymbol{\Omega}$. $\boldsymbol{D}$ and $\boldsymbol{\Omega}$ are the symmetric and skew parts of the velocity gradient. The coefficients may depend upon (s, $\boldsymbol{d}$, grad s, grad $\boldsymbol{d}$) and temperature. Equivalence between Equation (8) and the s evolution embedded in Equation (10) is obtained by setting $\beta_1 = 0$ and $\beta_2 = B_m / |\operatorname{grad} s|^{2-m}$, in which R depends upon grad s. We note here that such a choice implies hydrodynamic coupling in the evolution of degree of order s (8) and the dissipation (7) when flow is included, through the presence of the material time derivative, $\dot{s}$, which contains the velocity field.

However, since the non-convexity of interfacial energy involves grad s, it is possible that the evolution equation for s is numerically unstable in the cases where w is large. Recall the s evolution equation in Equation (8) is

$$\dot{s} = \frac{1}{B_m} |\operatorname{grad} s|^{2-m} \rho \left[-\frac{\partial \psi}{\partial s} + \operatorname{div} \left(\frac{\partial \psi}{\partial (\operatorname{grad} s)} \right) \right],$$

where ψ is taken as $W(\boldsymbol{d}, \operatorname{grad} \boldsymbol{d}, \boldsymbol{s}, \operatorname{grad} \boldsymbol{s})$. Then with the energy density given in Equation (11), $\frac{\partial \psi}{\partial \operatorname{grad} s}$ is calculated as

$$\begin{aligned} \left(\frac{\partial \psi}{\partial \operatorname{grad} s} \right)_i &= L_1 (\operatorname{grad} s)_i + \frac{\sigma_0}{|\operatorname{grad} s|} (\operatorname{grad} s)_i \\ &+ \frac{2\sigma_0 w}{|\operatorname{grad} s| |\boldsymbol{d}|^2} (d_i d_j s_{,j}) \\ &- \frac{\sigma_0 w \cos^2 \theta}{|\operatorname{grad} s|} (\operatorname{grad} s)_i + \text{other terms}, \end{aligned}$$

with θ being the angle between the interface normal direction and the tactoid interface, i.e. the angle between the directions grad s and $\boldsymbol{d}$. Thus, after substituting $\frac{\partial \psi}{\partial \operatorname{grad} s}$, we have

$$\begin{aligned} \dot{s} = C \Bigg\{ \operatorname{div} \Bigg[\Bigg(\Bigg(L_1 + \frac{\sigma_0}{|\operatorname{grad} s|} \Bigg) \boldsymbol{I} - w \Bigg(\frac{\sigma_0 \cos^2 \theta}{|\operatorname{grad} s|} \boldsymbol{I} \\ - \frac{2\sigma_0}{|\operatorname{grad} s| |\boldsymbol{d}|^2} \boldsymbol{d} \otimes \boldsymbol{d} \Bigg) \Bigg) \operatorname{grad} s \Bigg] \Bigg\} + \text{other terms}, \end{aligned}$$

where $C = \frac{|\operatorname{grad} s|^{2-m} \rho}{B_m}$. Denote the diffusion tensor $\boldsymbol{A}$ as

$$\begin{aligned} A = \left(L_1 + \frac{\sigma_0}{|\operatorname{grad} s|} \right) \boldsymbol{I} \\ - w \left(\frac{\sigma_0 \cos^2 \theta}{|\operatorname{grad} s|} \boldsymbol{I} - \frac{2\sigma_0}{|\operatorname{grad} s| |\boldsymbol{d}|^2} \boldsymbol{d} \otimes \boldsymbol{d} \right). \end{aligned}$$

Then, the s evolution equation can be written as

$$\dot{s} = C \operatorname{div}(\boldsymbol{A} \operatorname{grad} s) + \text{other terms}. \tag{13}$$

Since $\boldsymbol{d} \cdot \operatorname{grad} s$ is about 0 near the tactoid interface where grad s is non-zero (note that Equation (12) implies that $\boldsymbol{d}$ prefers to be perpendicular to grad s to minimise interfacial energy), the diffusion tensor $\boldsymbol{A}$ in div($\boldsymbol{A}$ grad s) may be negative definite depending on the relative magnitude of w, a potential cause for numerical instability.

In order to deal with this problem, we introduce a new field $\boldsymbol{p}$ representing the interfacial normal whose reciprocal magnitude roughly represents the width of the interface. The modified energy density with this new state descriptor is written as follows:

$$W(\boldsymbol{d}, \text{grad}\boldsymbol{d}, s, \text{grad}\, s, \boldsymbol{p}) = \frac{k_1}{2}\text{div}\,(d)^2 + \frac{k_2}{2}(\boldsymbol{d}\cdot\text{curl}(\boldsymbol{d}))^2 + \frac{k_2 - k_4}{2}(|\,\text{grad}\,\boldsymbol{d}|^2 - \text{div}\,(\boldsymbol{d})^2 - |\,\text{curl}(\boldsymbol{d})|^2) + \frac{k_3}{2}|d\times\text{curl}(\boldsymbol{d})|^2 + \frac{L_1}{2}|\,\text{grad}\, s - \boldsymbol{p}|^2 + f(s) + g(\boldsymbol{p}, \boldsymbol{d}),$$

where $f(s)$ is still the non-convex function of s in Equation (11) and $g(p, d)$ is a modified non-convex function representing interfacial energy given as

$$g(\boldsymbol{p}, \boldsymbol{d}) = |\boldsymbol{p}|\left[\sigma_0\left(\frac{1 + w(\boldsymbol{p}\cdot\boldsymbol{d})^2}{|\boldsymbol{p}|^2|\boldsymbol{d}|^2}\right)\right]. \tag{14}$$

By placing the non-convexity of the interfacial energy to be a function of $\boldsymbol{p}$ and $\boldsymbol{d}$, and elastically penalising the difference between $\boldsymbol{p}$ and grad$s$, we get a stable system for the phase transition model. The motivation for this change comes from phase-field like models of plasticity and phase transitions in solids that provide a practically useful way of avoiding the severe ill posedness that arises in problems which otherwise contain a non-convex energy contribution in the highest order derivative of a fundamental field (in the energy) being solved for. Physically, our assumption separates out the elasticity due to grad s from the interfacial energy, the latter assumed to be well-described here by the function g; close to equilibrium, at least, the elastic energy due to grad s is instead ascribed to deviations of grad s from the values of $\boldsymbol{p}$ at which the ground state of the interfacial energy g is attained (and not to the absolute magnitude of grad s), for each fixed value of $\boldsymbol{d}$. We also note that when $\boldsymbol{p}$ is perpendicular to $\boldsymbol{d}$, the interfacial energy is completely given by the isotropic contribution from g and our formulation does not 'double-count' interfacial energy in this situation if moreover grad s = $\boldsymbol{p}$.

With the modified energy density with the new state descriptor, the dissipation in Equation (6) (we ignore material motion for simplicity) can be written as

$$\int_V [\boldsymbol{\Lambda} : \boldsymbol{M}] - \rho\dot{\psi}]dv \geq 0$$

$$\Rightarrow \int_V \left[\boldsymbol{\Lambda}_{ij}\omega_{i,j} - \rho\frac{\partial W}{\partial d_i}\dot{d}_i - \rho\frac{\partial W}{\partial(d_{i,j})}\dot{d}_{i,j} - \rho\frac{\partial W}{\partial s}\dot{s} - \rho\frac{\partial W}{\partial(s_{,j})}\dot{s}_{,j} - \rho\frac{\partial W}{\partial p_i}\dot{p}_i\right]dv \geq 0.$$

Following the same procedure as in Section 3.2, we can verify that the dissipation is non-negative when $\dot{p}$ is in the direction of $-\frac{\partial W}{\partial \boldsymbol{p}}$. Thus, the dynamic evolution equation of the $\boldsymbol{p}$ field is given as

$$\dot{\boldsymbol{p}} = -Q\frac{\partial W}{\partial \boldsymbol{p}} = -Q\left[L_1(\boldsymbol{p} - \text{grad}\, s) + \frac{\partial g}{\partial \boldsymbol{p}}\right], \tag{15}$$

where Q is a material-dependent constant. An example of the advantage of the modified p model is discussed in Section 4.

The variables $\boldsymbol{d}$, s and the anchoring coefficient w are dimensionless. The variable p has dimension $[p] = Length^{-1}$. The physical dimensions of the parameters in the modified Oseen–Frank energy are $[k_1] = Force$, $[k_2] = Force$, $[k_3] = Force$, $[k_4] = Force$, $[L_1] = Force$ and $[\sigma_0] = Force \times Length^{-1}$. The physical dimensions of the coefficients C in Equation (13) and Q in Equation (15) are $[C] = Length^2 \times Time^{-1} \times Force^{-1}$ and $[Q] = Time^{-1} \times Force^{-1}$.

To non-dimensionalise the above parameters, we introduce the following dimensionless variables

$$\tilde{\boldsymbol{p}} = r\boldsymbol{p}; \quad \tilde{k}_i = \frac{k_i}{k_1}; \quad \tilde{L}_1 = \frac{L_1}{k_1}; \quad \tilde{\sigma}_0 = r\frac{\sigma_0}{k_1}; \quad \tilde{l} = \frac{l}{r},$$

where l is the dimensional length, $\tilde{l}$ is the dimensionless length and r is half of a typical tactoid size. In this work, we assume $k_1 = k_2 = k_3 = k$ (except in Section 5.1), $k_4 = 0$ and $L_1 = k$. Therefore, $\tilde{k}_1 = \tilde{k}_2 = \tilde{k}_3 = 1$, $\tilde{k}_4 = 0$ and $\tilde{L}_1 = 1$. The dimensionless $\tilde{\sigma}_0$ physically represents the ratio of the total surface energy and the total elastic energy, which would be $\frac{\sigma_0 r^2}{kr}$ for a three-dimensional nematic tactoid [36]. In this work, we assume r to be10 μm, based on the estimate of the long-axis length of a 'two-cusp tactoid' of 20 μm given in Ref. [1]. The physical parameters of LCLCs are adopted from Ref. [1] as follows: $k = 2 \times 10^{-12}N$ and $\sigma_0 = 10^{-4}J/m^2$, which implies $\tilde{\sigma}_0 = 500$. Since we do not focus on the evolution rates of s and $\boldsymbol{p}$, we assume that the time scales in s and $\boldsymbol{p}$ evolutions are similar by setting $Q = \frac{C}{r^2}$.

4. Tactoid equilibrium and phase transition results

We explore the capability of the phase transition model proposed in Sections 3.2 and 3.3 by solving tactoid equilibrium and dynamic problems. In static problems, both the initialised shapes from the Wulff construction and arbitrary initialised shapes are discussed. In addition, the nematic–isotropic phase transition and the formation of disclinations are also studied.

4.1. Tactoid static equilibrium

We discuss the results of tactoid equilibrium calculations with different anchor coefficients w. Based on the Wulff construction of equilibrium shapes of perfect crystals with the interfacial energy given in Equation (14), we can construct the equilibrium shapes of tactoids under the condition of constant surface area and a frozen director field [1,37–42]. In the static problem, we assume that the non-convex function $f(s)$ in the energy density has identical values at $s = 0$ and $s = 1$ characterising its minimum. Figure 3 shows the initialisations and the corresponding equilibrium results for various tactoids. The tactoid is initialised in the nematic $s = 1$ state and the matrix in the isotropic $s = 0$ phase. For fixed w, no large-scale evolution is seen to occur in tactoid shapes, but director reorientation occurs as the system seeks out a local minima.

The left column in Figure 3 shows the initialisations of the director field and tactoid shapes for different anchor coefficients w. The initialised tactoid shapes are calculated from the Wulff construction and the director fields start from a uniform unit vector field where $s = 1$. The right column in Figure 3 is the equilibrium configurations corresponding to the initialisations. It shows that with increasing w, the single tactoid shape started from the Wulff construction transforms from sphere-like to ellipse-like shape. In all cases, given the interfacial energy in Equation (14), the director field tends to be perpendicular to the interface normal grad s.

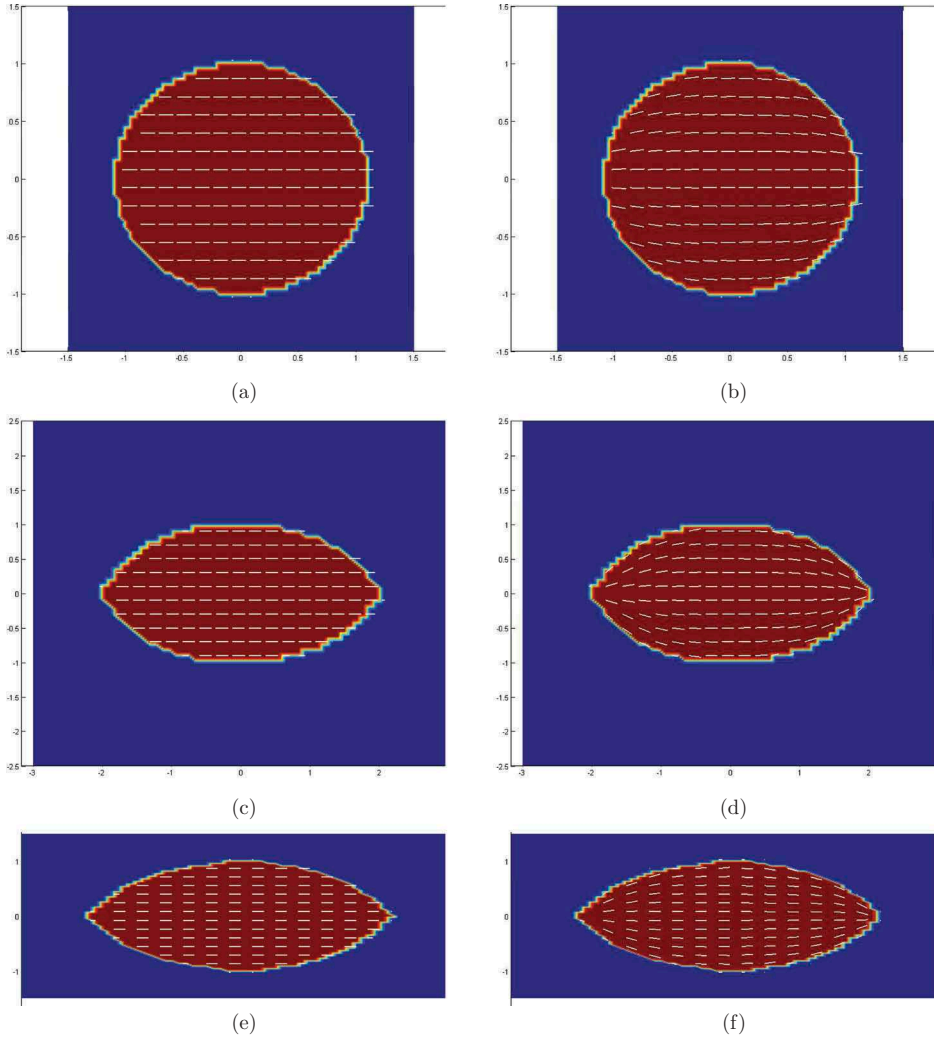

Figure 3. (Colour online) Initialisations and equilibria of tactoid static problems with different anchor coefficients. The red colour represents $s = 1$, the blue colour represents $s = 0$ and the white dash lines represent the director field. The tactoid initialisations are calculated from the Wulff construction. (a) The initialized tactoid shape and director field with w = 0.1. (b) The equilibrium of the tactoid shape and director field with w = 0.1. (c) The initialized tactoid shape and director field with w = 1. (d) The equilibrium of the tactoid shape director field with w = 1. (e) The initialized tactoid shape and director field with w = 2. (f) The equilibrium of the tactoid shape and director field with w = 2.

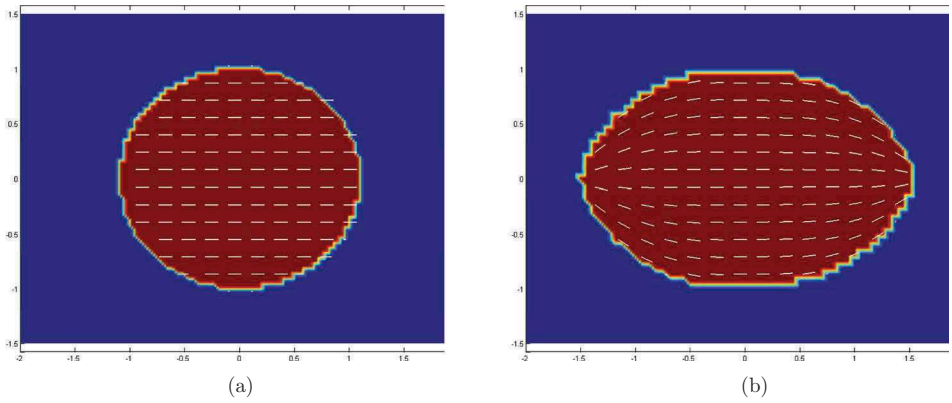

Figure 4. (Colour online) The initialised tactoid shape is a sphere with $w = 2.5$. At the equilibrium, the spherical tactoid transforms to an ellipse-like tactoid and the director field evolves. (a) The spherical initialized tactoid shape with w = 2:5. (b) The equilibrium of the tactoid shape and director field with w = 2.5.

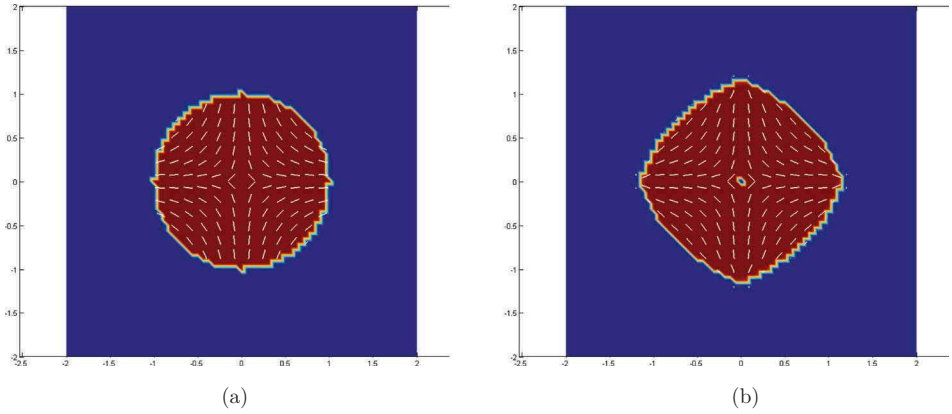

Figure 5. (Colour online) A spherical tactoid transforms to a rounded-square tractoid with $w = 1.5$ and a negative disclination of strength -1. (a) The spherical initialized tactoid shape with w = 1.5 and the initialized director field corresponds to a negative disclination of strength −1. (b) The tactoid shape and director field at equilibrium.

Recall that we introduced a new field $\boldsymbol{p}$ and discussed the theoretical motivation behind it in Section 3.3. In Figure 3(f), the anchor coefficient w is set to be large, $w = 2$. In this case, without introducing the $\boldsymbol{p}$ field, the computation is unstable and an equilibrium could not be found. With the introduced field $\boldsymbol{p}$, this case can be solved with result shown in Figure 3(f). The results of various tactoid shapes show that cusps are recovered in our model, matching with experimental observations [1].

The initialised tactoid shapes in Figure 3 are based on the Wulff construction. The determined shape from the Wulff procedure depends on the value of w. In addition, the calculation shown in Figure 4 explores the capability of the proposed model with a specified w and an arbitrary initialised shape. In Figure 4, w is assumed to be 2.5 but the initialised tactoid shape is a sphere which clearly does not match with the Wulff construction. Figure 4(a) is the initialisation of the tactoid shape and the director field and Figure 4(b) is the corresponding computed equilibrium state. It shows that the initialised spherical tactoid shape transforms to an elliptic shape due to the high value of w.

Figure 5 shows another example with a non-Wulff-constructed initialised shape in which $w = 1.5$ and the director field are prescribed with a singularity corresponding to a negative disclination of strength -1. Figure 5(a) is the initialised spherical tactoid shape and the director field with the discontinuity at the centre of the tactoid. Figure 5(b) shows the final equilibrium state indicating that the tactoid transforms to a rounded square, and a negative disclination (with its core in the isotropic phase $s = 0$) exists at the centre of the tactoid.

4.2. Dynamics of tactoids interaction

The interaction between two tactoids located close to each other is computed. Two spherical tactoids are

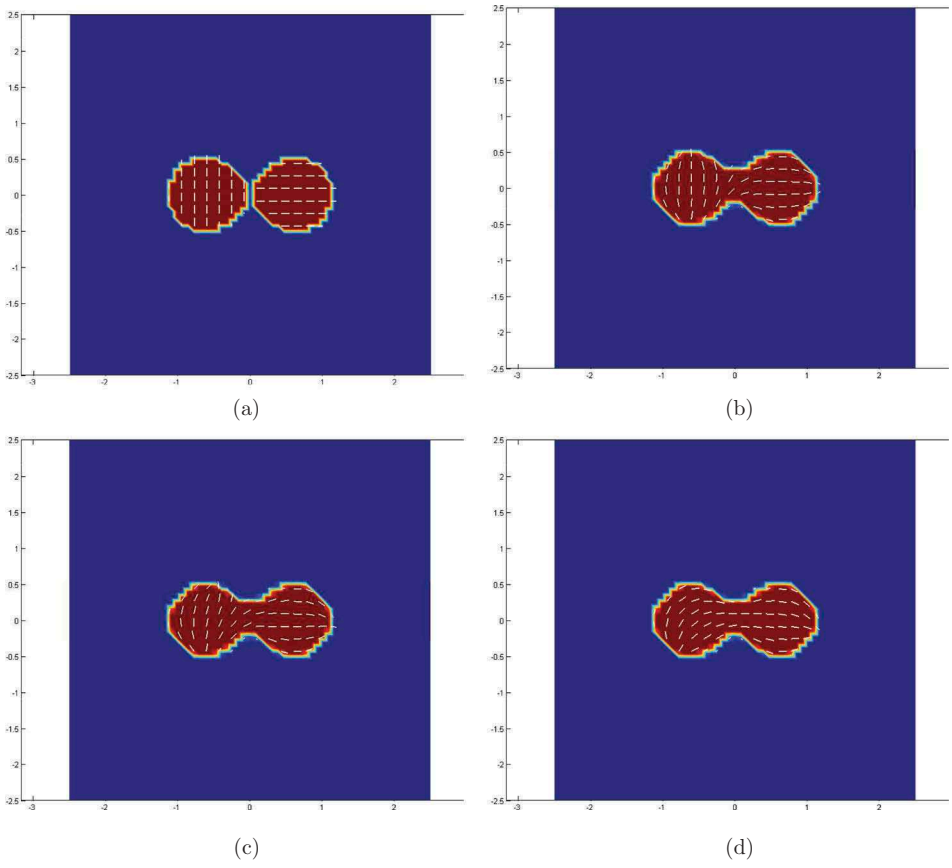

Figure 6. (Colour online) Interaction between two tactoids. These two tactoids tend to merge and the director field evolves. (a) The initialized tactoid shape and director field for two tactoids interaction. (b) Two tactoids begin to merge and the director evolves. (c) The director keeps evolving. (d) The equilibrium of two tactoid interaction.

initialised with different director orientations, as shown in Figure 6(a). Since these two tactoids are located very close to each other, they are expected to interact with each other. As the calculation progresses, the tactoids begin to merge and the director field evolves to minimise the total energy, as shown in Figure 6.

In this calculation, $m = 0$ and the barrier of the non-convex function $f(s)$ in the energy density between $s = 0$ and $s = 1$ is low. The shape of the non-convex function $f(s)$ is shown in Figure 7. In the tactoid evolution, the effect of m is critical.

- For the static equilibrium problem of a single tactoid, with higher barrier of $f(s)$, a single tactoid will evolve to its equilibrium state with no problem.
- For the static equilibrium problem, with a low barrier of $f(s)$, and $m = 2$, the single tactoid will diffuse into the isotropic matrix and the interface cannot maintain its shape. On the other hand, with a low barrier of $f(s)$, and $m = 0$, the single tactoid will evolve to its equilibrium state.

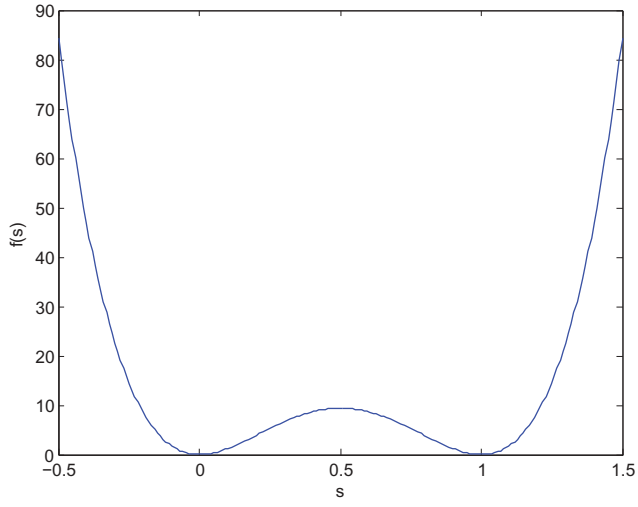

Figure 7. (Colour online) The shape of $f(s)$ used in the two tactoids interaction calculation. The barrier between two wells at $s = 0$ and $s = 1$ is low.

- For dynamic problems, such as the tactoid interaction discussed in this section, the tactoids are not able to merge with a high barrier in $f(s)$.

- With a low barrier of $f(s)$ as applied in this calculation and $m = 0$, the tactoids are able to move, expand or merge.

To understand the reason for the effect of the energy barrier and m value, recall that the s evolution equation is given as

$$\dot{s} = \frac{1}{B_m} |\text{grad}\, s|^{2-m} \rho \left[-\frac{\partial \psi}{\partial s} + \text{div} \left(\frac{\partial \psi}{\partial (\text{grad}\, s)} \right) \right].$$

In the case of high barrier of $f(s)$, regardless of m, s can barely evolve from their well values because of the high value of the 'resisting force' from $\frac{\partial \psi}{\partial s}$. In the case of low barrier of $f(s)$, with $m = 2$, there is no impediment for s to evolve out of the isotropic well. In the case of low barrier and with $m = 0$, although the barrier of $f(s)$ is low, s cannot evolve where grad s is 0.

This is analogous to a problem in Ref. [22], where the dissipative dynamic behaviour of disclinations in nematic LCs is studied. By observing the effect of m on low barrier cases, we show that the dynamic model based on *kinematics* and thermodynamics is important for modelling dissipative dynamics.

4.3. Phase transition

We now discuss a problem of evolving phase transition across the whole domain. Three tactoids with different director orientations are initialised as shown in Figure 8 (a). The non-convex part $f(s)$ in the energy density is assumed to prefer the nematic phase, indicating the well at $s = 1$ is lower than the well at $s = 0$. The preference of the nematic phase of $f(s)$ indicates that the LC should transit from the isotropic to the nematic phase. Figure 8 (b–d) shows snapshots at different times during the phase transition. As time increases, the tactoids expand and merge. In Figure 8(d), a strength -1 disclination is formed inside the bulk which matches with experimental observations [1].

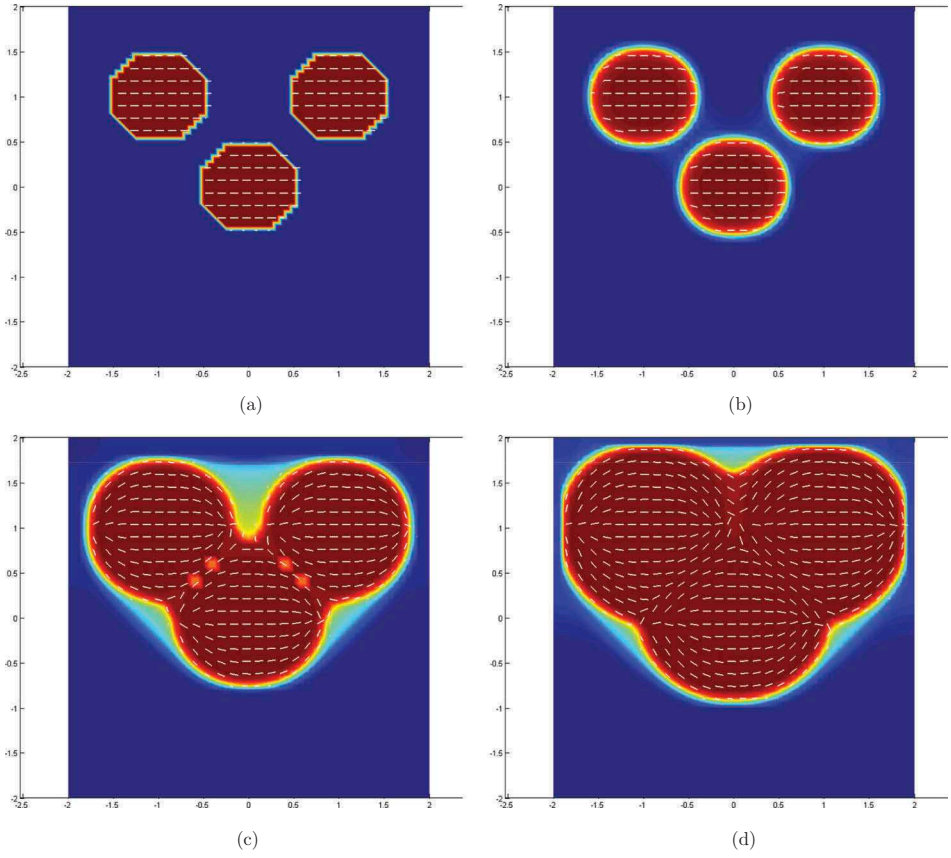

Figure 8. (Colour online) Snapshots of isotropic–nematic phase transition at different times. As the calculation progresses, the tactoids expand, merge and a strength -1 disclination is formed inside the bulk. (a) The initialized tactoid shape and director field. Three spherical tactoids with same director fields are initialized. (b) The tactoid shapes and director field at t = 0.1. Three tactoids expand. (c) The tactoid shapes and director field at t = 0.2. The tactoids begin to merge. (d) The tactoid shapes and director field at t = 0.5. A strength −1 disclination is formed inside the bulk.

5. Effect of material parameters on tactoid equilibria

Since the energy proposed in this model is non-convex and the equilibrium of the tactoid and the director field depend on the interfacial energy and the Frank constants, it is of interest to explore tactoid equilibria as a function of material parameters.

5.1. Frank constants k_{11} and k_{33}

We consider two cases, $k_{11} > k_{33}$ (splay more expensive than bend) or $k_{11} < k_{33}$ (bend more expensive than splay). In one case, we assume k_{11} is five times larger than k_{33}; in the other, we assume k_{33} is five times larger than k_{11}. The tactoid shape is initialised as a sphere in both cases.

Figures 9 and 10 show the initial configuration and the equilibrium state for both cases. In Figure 9, k_{11} is larger than k_{33} and the director in the equilibrium tends to be perpendicular to the tactoid interface normal direction and bend is preferred over splay. On the other hand, in Figure 10, the director tends to be parallel to the interface normal direction with splay preferred over bend. The difference between these two results indicates that the relationship between k_{11} and k_{33} is crucial to the interaction between the director and the tactoid interface, which is also discussed in the experiments reported in Ref. [17].

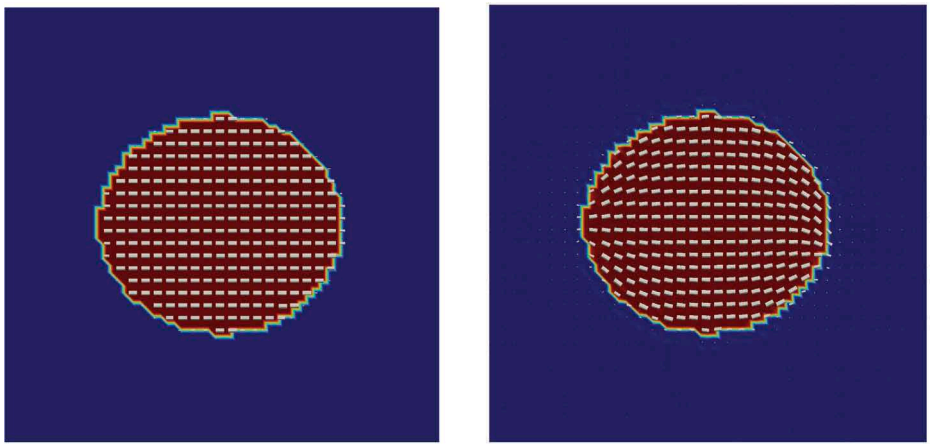

(a) (b)

Figure 9. (Colour online) The initialisation and equilibrium configuration of the tactoid and director field in the case where $k_{11} > k_{33}$. Since splay is more expensive than bend, the director field tends to be perpendicular to the interface normal. (a) The initialized tactoid shape and director field. (b) The tactoid shape and director field at the equilibrium.

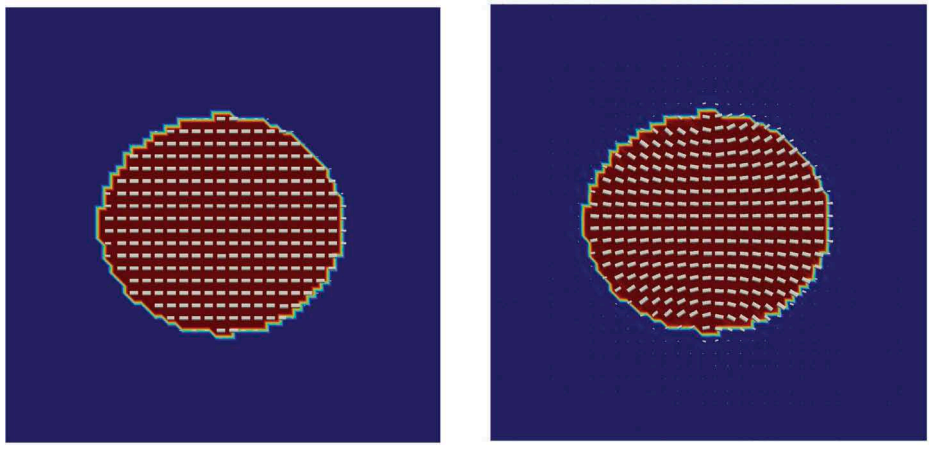

(a) (b)

Figure 10. (Colour online) The initialisation and equilibrium configuration of the tactoid and director field in the case where $k_{11} < k_{33}$. Since bend is more expensive than splay, the director field tends to be parallel to the interface normal. (a) The initialized tactoid shape and director field. (b) The tactoid shape and director field at the equilibrium.

5.2. Effect of interfacial energy barrier on tactoid shape

Recall that in Equation (14), the interfacial energy is given in terms of the cosine of the angle θ between $\boldsymbol{p}$ representing the normal of the interface and the director field $\boldsymbol{d}$, which has a minimum at $\theta = \frac{\pi}{2}$. However, this approximation of the interfacial energy is only valid when the angle θ is close to $\frac{\pi}{2}$. We now assume an interfacial energy characterised by a fourth-order polynomial with two local minima and a local maximum as shown in Figure 11. Such a form of the surface anchoring potential was first introduced by Sluckin and Poniewierski [43] and applied for the description of interfacial effects in LCLCs by

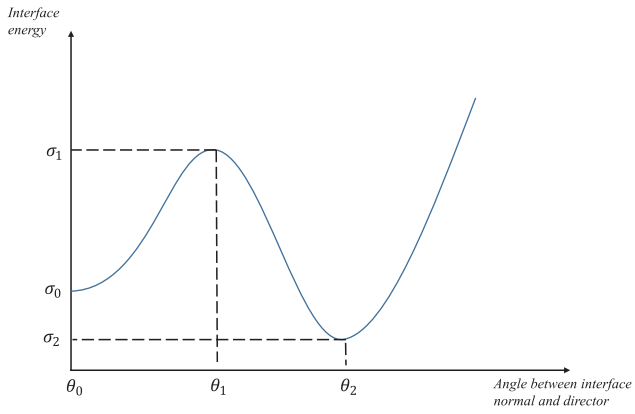

Figure 11. (Colour online) The shape of the interfacial energy with two local minimal and a local maximal.

σ_0	σ_1	σ_2	*Initialized Configuration*	*Energy*	*Equilibrium Configuration*	*Energy*
0	0	0	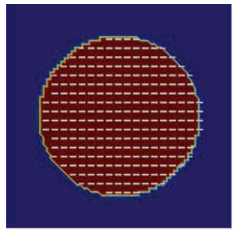	1	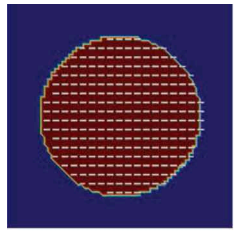	0.86
0	2	0	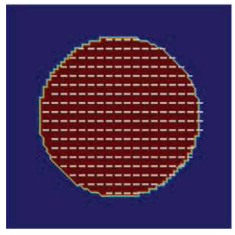	1.63	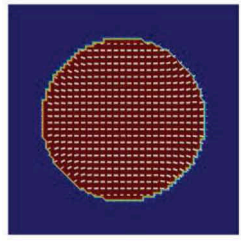	1.27
0	1	0.5	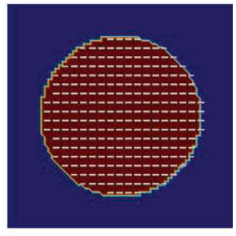	1.59	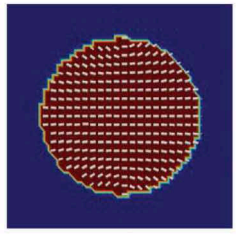	1.08
0	5	0.5	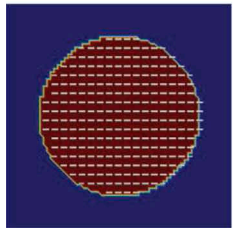	2.86	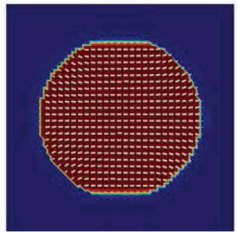	1.93

Figure 12. (Colour online) The initialisations and static equilibriums of the tactoid shape and director field given different interfacial energy parameters in the cases where $\sigma_0 = \sigma_2$ and $\sigma_0 < \sigma_2$. The total energy for each case is normalised by the energy value for the initialisation of the case where $\sigma_0 = \sigma_1 = \sigma_2 = 0$.

Nazarenko et al. [19]. $\theta_0 = 0$ is where one local minimum occurs, θ_1 is the location of the local maximum and $\theta_2 = \frac{\pi}{2}$ is the location of the other local minimum. σ_0, σ_1 and σ_2 are the interfacial energy values at θ_0, θ_1 and θ_2, respectively.

It is clear that the energy barrier between the two wells θ_0 and θ_2, as well as the values of σ_0 and σ_1, will influence the equilibrium state of the director field and the tactoid shape. Here, we explore the relationship between the energy values of local maximum, as well as local minima, and the equilibrium of the director field. We assume $\theta_1 = \frac{\pi}{4}$ and change σ_0, σ_1 and σ_2.

Figures 12 and 13 show the initialisations and equilibria of tactoid shapes and their director fields given different interfacial energy parameters. In the first row of Figure 12, σ_0, σ_1 and σ_2 are set to be 0 so the interfacial energy will be zero at any angle between the director and the interface normal. Thus, the director field in the equilibrium is the same as the initialisation. The second row shows the initialised configuration and static equilibrium corresponding to a higher σ_1 values. Since the energy barrier between θ_0 and θ_2 is high, the director field tends to move to its local minimum, namely some points being parallel to the interface normal and some points being perpendicular to the interface normal. The last two rows in Figure 12 show different equilibria with the increasing energy barrier σ_1 in the case where $\sigma_0 < \sigma_2$. With low barrier $\sigma_1 = 1$, the director field can evolve to the lower well at θ_0, thus the director field in the equilibrium is parallel to the interface normal. With high barrier $\sigma_1 = 5$, the director field cannot pass the local maximum between θ_0 and θ_2 and evolve to its local minimum in the equilibrium. In addition, Figure 12 shows the total energy for each case, which are normalised by the total energy of the case where $\sigma_0 = \sigma_1 = \sigma_2 = 0$.

Similarly, Figure 13 shows the results with increasing energy barrier σ_1 in the case where $\sigma_0 > \sigma_2$. With low barrier $\sigma_1 = 1$, the director field can evolve to the lower well at θ_2, and the director field in the equilibrium is perpendicular to the interface normal. With high barrier $\sigma_1 = 5$, the director field can only evolve to its local minimum in the equilibrium. Figure 13 also

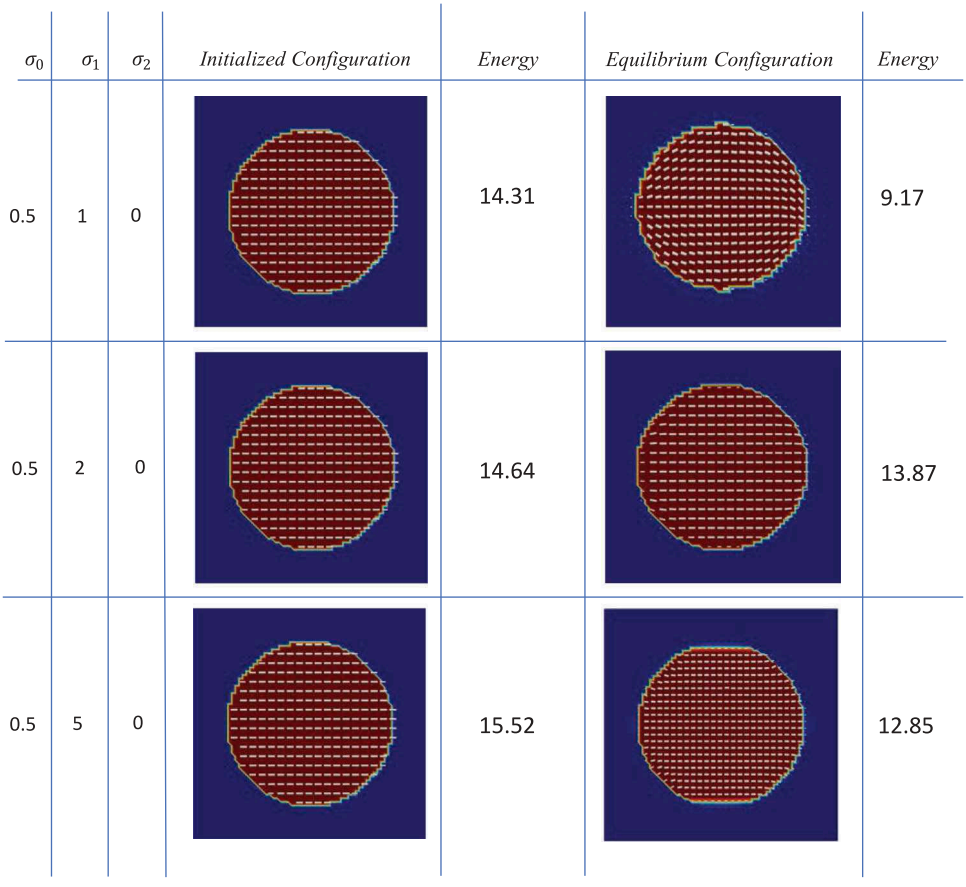

Figure 13. (Colour online) The initialisations and static equilibriums of the tactoid shape and director field given different interfacial energy parameters in the case where $\sigma_0 > \sigma_2$. The total energy for each case is normalised by the energy value for the initialisation of the case where $\sigma_0 = \sigma_1 = \sigma_2 = 0$.

shows the total energy for each case, and the values of the total energy are normalised by the one of the case where $\sigma_0 = \sigma_1 = \sigma_2 = 0$.

6. Conclusion

A model based in continuum kinematics and thermodynamics is derived for LCLC I–N phase transition dynamics. By adopting the order parameter s in Ref. [26] to represent different phase states, an evolution equation of s is proposed and discussed. The main difference between our model and Ericksen's model in Ref. [26] is that the model in this work starts from a kinematic 'tautology' with transparent physical/geometric motivation. The evolution of the director field is described by the formulation in Ref. [34]. A new field $\boldsymbol{p}$ is introduced in the energy density to resolve the instabilities in the s evolution resulting from the non-convex interfacial energy when phrased only in terms of grad s and $\boldsymbol{d}$.

Both static equilibrium and dynamic tactoid behaviours are studied, including tactoid static microstructures from different initialised shapes, tactoid interactions and I–N phase transitions. The significance of the introduced evolution equation for s is discussed in the context of describing tactoid dynamic behaviours. A parametric study is performed to explore the effect of nematic elastic constants (splay and bend) and the interfacial energy parameters on the interaction between the tactoid interface normal and the director field.

Acknowledgements

Support from the NSF DMREF programme through grant DMS1434734 is gratefully acknowledged. ODL also acknowledges support from grant NSF DMS-1434185.

Disclosure statement

No potential conflict of interest was reported by the authors.

Funding

This work was supported by the National Science Foundation: [Grant Numbers DMS1434185 and DMS1434734].

References

[1] Kim Y-K, Shiyanovskii SV, Lavrentovich OD. Morphogenesis of defects and tactoids during isotropic–nematic phase transition in self-assembled lyotropic chromonic liquid crystals. J Phys. 2013;25 (40):404202.

[2] Lydon J. Chromonic liquid crystalline phases. Liq Cryst. 2011;38(11–12):1663–1681.

[3] Collings PJ, Goldstein JN, Hamilton EJ, et al. The nature of the assembly process in chromonic liquid crystals. Liq Cryst Rev. 2015;3(1):1–27.

[4] Park HS, Lavrentovich OD. Lyotropic chromonic liquid crystals: emerging applications. In: Quan Li, editor. Liquid crystals beyond displays: chemistry, physics, and applications. Chapter 14. Hoboken, NJ: John Wiley & Sons; 2012.

[5] Nastishin YA, Liu H, Shiyanovskii SV, et al. Pretransitional fluctuations in the isotropic phase of a lyotropic chromonic liquid crystal. Phys Rev E. 2004;70 (5):051706.

[6] Park H-S, Kang S-W, Tortora L, et al. Condensation of self-assembled lyotropic chromonic liquid crystal sunset yellow in aqueous solutions crowded with polyethylene glycol and doped with salt. Langmuir. 2011;27(7):4164–4175.

[7] Tortora L, Park H-S, Kang S-W, et al. Self-assembly, condensation, and order in aqueous lyotropic chromonic liquid crystals crowded with additives. Soft Matter. 2010;6:4157–4167.

[8] Nastishin YA, Liu H, Schneider T, et al. Optical characterization of the nematic lyotropic chromonic liquid crystals: light absorption, birefringence, and scalar order parameter. Phys Rev E. 2005 Oct;72:041711.

[9] Tortora L, Lavrentovich OD. Chiral symmetry breaking by spatial confinement in tactoidal droplets of lyotropic chromonic liquid crystals. Proc Natl Acad Sci. 2011;108 (13):5163–5168.

[10] Kleman M, Laverntovich OD. Soft matter physics: an introduction. Berlin: Springer Science & Business Media; 2007.

[11] Chuang I, Durrer R, Turok N, et al. Cosmology in the laboratory: defect dynamics in liquid crystals. Science. 1991;251(4999):1336–1342.

[12] Bowick MJ, Chandar L, Schiff EA, et al. The cosmological kibble mechanism in the laboratory: string formation in liquid crystals. Science. 1994;263(5149):943–945.

[13] Vachaspati T. Formation of topological defects. Phys Rev D. 1991;44(12):3723–3729.

[14] Volovik GE, Lavrentovich OD. Topological dynamics of defects: boojums in nematic drops. Zh Eksp Teor Fiz. 1983;85(6): 1159–1167. pp. 1997–2010, 1983./Sov. Phys. JETP, v.58.

[15] Zhou S, Nastishin YA, Omelchenko MM, *et al*. Elasticity of lyotropic chromonic liquid crystals probed by director reorientation in a magnetic field. Phys Rev Lett. 2012;109(3):037801.

[16] Zhou S, Neupane K, Nastishin YA, et al. Elasticity, viscosity, and orientational fluctuations of a lyotropic chromonic nematic liquid crystal disodium cromoglycate. Soft Matter. 2014;10:6571–6581.

[17] Zhou S, Cervenka AJ, Lavrentovich OD. Ionic-content dependence of viscoelasticity of the lyotropic chromonic liquid crystal sunset yellow. Phys Rev E. 2014;90.

[18] Schneider T, Artyushkova K, Fulghum JE, et al. Oriented monolayers prepared from lyotropic chromonic liquid crystal. Langmuir. 2005;21(6):2300–2307.

[19] Nazarenko VG, Boiko OP, Park H-S, et al. Surface alignment and anchoring transitions in nematic

lyotropic chromonic liquid crystal. Phys Rev Lett. 2010;105(1):017801.
[20] Zhou S, Shiyanovskii SV, Park H-S, et al. Fine structure of the topological defect cores studied for disclinations in lyotropic chromonic liquid crystals. Nat Commun. 2017;8:14974.
[21] Kibble TWB. Topology of cosmic domains and strings. J Phys A Math Gen. 1976;9(8):1387–1398.
[22] Zhang C, Zhang X, Acharya A, et al. A non-traditional view on the modeling of nematic disclination dynamics. Q Appl Math. 2016;75(2):309–357.
[23] Popa-Nita V, Sluckin TJ. Kinetics of the nematic-isotropic interface. J Phys II. 1996;6(6):873–884.
[24] Grollau S, Abbott NL, De Pablo JJ. Spherical particle immersed in a nematic liquid crystal: effects of confinement on the director field configurations. Phys Rev E. 2003;67(1):011702.
[25] Virga EG. Variational theories for liquid crystals. Vol. 8. Boca Raton, FL: CRC Press; 1995.
[26] Ericksen JL. Liquid crystals with variable degree of orientation. Arch Ration Mech Anal. 1991;113(2):97–120.
[27] Frank FC. I. Liquid crystals. On the theory of liquid crystals. Discuss Faraday Soc. 1958;25:19–28.
[28] Oseen CW. The theory of liquid crystals. Trans Faraday Soc. 1933;29(140):883–899.
[29] Hardt R, Kinderlehrer D, Lin F-H. Existence and partial regularity of static liquid crystal configurations. Commun Math Phys. 1986;105(4):547–570.
[30] Leslie FM. Continuum theory for nematic liquid crystals. Continuum Mech Therm. 1992;4(3):167–175.
[31] Acharya A, Dayal K. Continuum mechanics of line defects in liquid crystals and liquid crystal elastomers. Q Appl Math. 2013;72(1):33–64.
[32] Ericksen JL. Conservation laws for liquid crystals. Trans Soc Rheol. 1961;5(1):23–34.
[33] Stewart IW. The static and dynamic continuum theory of liquid crystals: a mathematical introduction. Boca Raton, FL: CRC Press; 2004.
[34] Walkington NJ. Numerical approximation of nematic liquid crystal flows governed by the Ericksen-Leslie equations. ESAIM: Math Modelling Numer Anal. 2011;45(3):523–540.
[35] Rapini A, Papoular M. Distorsion d'une lamelle nématique sous champ magnétique conditions d'ancrage aux parois. J Phys Colloq. 1969;30(C4):C4–56.
[36] Lavrentovich OD. Topological defects in dispersed words and worlds around liquid crystals, or liquid crystal drops. Liq Cryst. 1998;24(1):117–126.
[37] Burton WK, Cabrera N, Frank FC. The growth of crystals and the equilibrium structure of their surfaces. Philos Trans Royal Soc A. 1951;243(866):299–358.
[38] Landau LD, Lifshits EM. Course of theoretical physics. Stat Phys. 1964;5.
[39] Oswald P, Pieranski P. Nematic and cholesteric liquid crystals: concepts and physical properties illustrated by experiments. Boca Raton, FL: CRC press; 2005.
[40] Wheeler AA. Phase-field theory of edges in an anisotropic crystal. Proc Royal Soc A. 2006;462: 3363–3384. The Royal Society.
[41] Khare SV, Kodambaka S, Johnson DD, et al. Determining absolute orientation-dependent step energies: a general theory for the Wulff-construction and for anisotropic two-dimensional island shape fluctuations. Surf Sci. 2003;522(1–3):75–83.
[42] Nozi'eres P. Shape and growth of crystals. Solids Far Equilib. 1992;56(2):1–154.
[43] Sluckin TJ, Poniewierski A. Fluid interfacial phenomena. C. Croxton, editor. Chichester: John Wiley and Sons; 1986.